LAWRENCE
LIVERMORE
NATIONAL
LABORATORY

LLNL-CONF-651630

Predictions for p+Pb Collisions at \sqrt sNN = 5 TeV: Expectations vs. Data

R. Vogt

March 11, 2014

Hard Probes 2013
Stellenbosch, South Africa
November 4, 2013 through November 8, 2013

Disclaimer

Available online at www.sciencedirect.com
ScienceDirect
Nuclear Physics A 00 (2014) 1–4
Nuclear Physics A

Predictions for p+Pb Collisions at $\sqrt{s_{NN}}$ = 5 TeV: Expectations vs. Data

R. Vogt

Physics Division, Lawrence Livermore National Laboratory, Livermore, CA 94551, USA
Physics Department, University of California, Davis, CA 95616, USA

Abstract

Recently a compilation of predictions for charged hadron, identified light hadron, quarkonium, photon, jet and gauge boson production in p+Pb collisions at $\sqrt{s_{NN}}$ = 5 TeV was made available [1]. Here the predictions are compared to the data so far available.

Keywords:
cold nuclear matter effects, charged particle production, J/ψ

1. Introduction

Members and friends of the JET Collaboration calculated predictions for the $\sqrt{s_{NN}}$ = 5.02 TeV p+Pb run at the LHC in the winter of 2013. Predictions were collected for charged hadrons; identified particles such as π^0, $K^{\pm}$, and $p/\overline{p}$; photons; jets; J/ψ; and gauge bosons. The observables included individual distributions, ratios such as $R_{p\mathrm{Pb}}$, and correlation functions. The paper in which these predictions were compiled [1] was submitted to International Journal of Modern Physics E and to arXiv.org before the p+Pb run began. This paper presents the confrontation of the predictions with data available by the time of Hard Probes 2013. We focus on charged hadron multiplicities and J/ψ here.

The particle multiplicities, p_T distributions and nuclear modification factors, $R_{p\mathrm{Pb}}$, in p+Pb collisions can be calculated in several different approaches. These are briefly outlined here. All involve some parameters tuned at a specific energy to predict results for other energies. For details and model references see Ref. [1].

Event generators determine multiplicities from their models of soft particle production followed by fragmentation and hadronization. Hard particle production is typically based on a pp generator such as `PYTHIA`. Examples include `HIJING`, `HIJINGB`$\overline{\mathtt{B}}$ and `AMPT`.

Perturbative QCD approaches involving collinear factorization at leading and next-to-leading order typically require a minimum p_T for validity, making estimates of total multiplicity difficult. However, above this minimum p_T, they can calculate the p_T distributions and modification factors. These calculations differ in the cold nuclear matter effects employed and the parameters used. Nuclear shadowing is generally included, as is isospin, differences due to the proton and neutron number of the target nucleus (most important for Drell-Yan and gauge boson production). Broadening of the p_T distributions in cold matter and medium-induced energy loss are also often included.

Email address: vogt@physics.ucdavis.edu (R. Vogt)

A more first-principles QCD approach that can provide an estimate of the total multiplicity is the color glass condensate (CGC). This provides a saturation-based description of the initial state in which nuclei in a high-energy nuclear collision appear to be sheets of high-density gluon matter. In this approach, gluon production can be described by $k_{\rm T}$-factorization which assumes an ordering in intrinsic transverse momentum rather than momentum fraction x, as in collinear factorization. The unintegrated gluon density associated with k_T factorization is related to the color dipole forward scattering amplitude which satisfies the JIMWLK evolution equations. In the large N_c limit, the JIMWLK equations simplify to the Balitsky-Kovchegov (BK) equation, a closed-form result for the rapidity evolution of the dipole amplitude. The running coupling corrections to the leading log BK equation, rcBK, have been phenomenologically successful in describing the rapidity/energy evolution of the dipole. The initial condition still needs to be modeled, generally employing the McLerran-Venugopalan model with parameters constrained by data. The impact parameter dependent dipole saturation model (IP-Sat) is a refinement of the dipole saturation model that reproduces the correct limit when the dipole radius $r_T \to 0$. It includes power corrections to the collinear DGLAP evolution and should be valid where logs in Q^2 dominate logs of x.

2. Charged Hadrons

In our compilation [1], it was shown that the charged particle pseudorapidity distributions, $dN_{\rm ch}/d\eta$, exhibited a considerably steeper slope than the data, particularly for η in the direction of the lead nucleus. Further communication with Albacete and Dumitru [7] showed that $dN_{\rm ch}/d\eta$ depends strongly on the $y \longrightarrow \eta$ transformation. The rcBK calculation depends on this Jacobian, not uniquely defined in the CGC framework. It is necessary to assume a fixed minijet mass, related to the pre-hadronization/fragmentation stage. Thus, in Ref. [1], they assumed the same transformation for pp and p+Pb collisions. The result on the left-hand side of Fig. 1 shows the dependence of $dN_{\rm ch}/d\eta$ on the Jacobian transformation. The open and filled squares represent the original result [1] while the filled triangles are based on a Jacobian with the hadron momentum modified by $\Delta P(\eta) = 0.04\eta[(N_{\rm part}^{\rm proj} + N_{\rm part}^{\rm targ})2 - 1]$. The results are essentially identical in the proton direction but differ considerably in the direction of the lead beam. The difference shows the sensitivity of this result to the mean mass and p_T of the unidentified final-state hadrons.

The right-hand side of Fig. 1 contrasts the centrality dependence calculated by two rather different methods: the default `AMPT` model [2] and the b-CGC approach [3]. While the two calculations do not display exactly the same centrality bins, the $20-40\%$, $40-60\%$, $60-80\%$ and the centrality-averaged minimum bias (min bias) results are shown for both calculations.

In `AMPT`, the centrality in p+Pb collisions is defined according to the number of charged hadrons within $|\eta| < 1$ in the center of mass frame. The $40-60\%$ centrality bin gives a distribution that is very close to the min bias result, in particular on the proton side. The most central bin is the most asymmetric distribution, as well as the largest in magnitude. On the other hand, the distribution for the $80-100\%$ centrality bin is symmetric around $\eta_{\rm cm} = 0$ and lower in magnitude than the pp distribution. The pp events are min bias, including diffractive events.

The b-CGC approach, employing k_T factorization, is shown for several centrality bins as well as for minimum-bias collisions [3]. The impact parameter dependence of the saturation model is crucial for defining the collision centrality. The largest asymmetry in the multiplicity distribution is observed in more central collisions while, for peripheral collisions such as the $60-80\%$ bin, the system becomes more similar to that of pp collisions. A fixed minijet mass equal to the current-quark mass is assumed. Since the minijet mass is related to pre-hadronization/hadronization stage and cannot be obtained from saturation physics, it was fixed by fitting lower energy minimum-bias data. In very peripheral collisions, where the system becomes more similar to symmetric pp collisions, this assumption is less reliable. More importantly, k_T factorization is only proven in asymmetric pA collisions at small x. Thus this calculation is limited to $|\eta_{\rm cm}| \leq 3$.

The results of the two calculations are somewhat similar in shape although, when directly compared in the same centrality bins, the `AMPT` multiplicities tend to be slightly higher while the b-CGC results have a somewhat stronger dependence on η. In the most peripheral comparable bin, $60-80\%$, the b-CGC result is almost independent of η while the `AMPT` result is somewhat lower and still shows a dip at midrapidity between the proton and lead directions. The preliminary ATLAS centrality-dependent multiplicity was presented here [4]. In the more peripheral bins, the results are compatible with both calculations albeit independent of η. In the most central bins, $0-1\%$ and $1-5\%$, a relatively strong η dependence is observed.

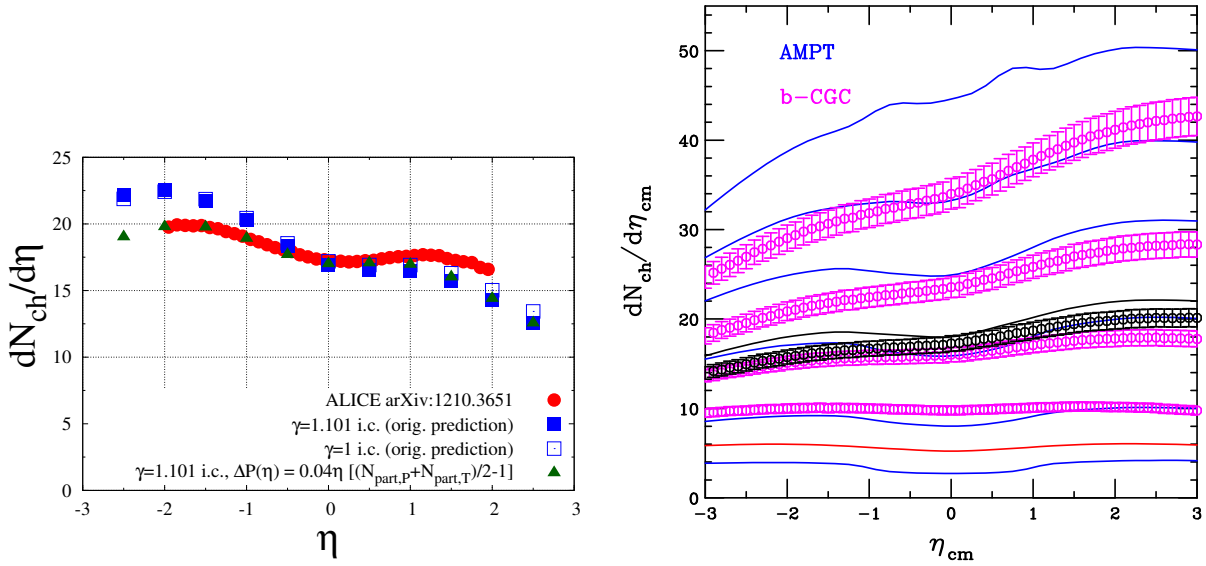

Figure 1. (Left) Charged particle pseudorapidity distribution at $\sqrt{s_{NN}}$ = 5.02 TeV as a function of η with and without the adjusted Jacobian. In this figure the proton beam moves toward positive rapidity. Courtesy of Albacete *et al.* [7]. (Right) Charged particle pseudorapidity distributions in the center of mass frame of p+Pb collisions at various centralities for AMPT [2] (lines, from top to bottom 0-10%, 10-20%, 20-40%, 40-60%, 60-80% and 80-100%; black, min bias; and pp, red) and the b-CGC saturation model [3] (points, from top to bottom, 0-20%, 20-40%, 40-60% and 60-80%; black, min bias). In these calculations the lead beam moves toward positive rapidity.

3. J/ψ

The J/ψ results from ALICE [5] and LHCb [6] are in similar rapidity windows, $2.5 < y_{\rm cm} < 4$ for ALICE and $2.5 < y_{\rm cm} < 5$ for LHCb in symmetric (pp and AA) collisions. Although the muon spectrometers for both experiments are only on one side of the collision point, results were obtained forward and backward of midrapidity by switching the beam direction and running both p+Pb and Pb+p collisions. Due to the rapidity shift in asymmetric collisions, the acceptances of the two detectors in the collision center of mass was shifted to $2.03 < y_{\rm cm} < 3.53$ at forward rapidity and $-4.46 < y_{\rm cm} < -2.96$ at backward rapidity for ALICE and $1.5 < y_{\rm cm} < 4$ at forward rapidity and $-5 < y_{\rm cm} < -2.5$ at backward rapidity for LHCb. The regions of overlap between the forward and backward rapidity regions are $2.96 < |y_{\rm cm}| < 3.53$ for ALICE and $2.5 < |y_{\rm cm}| < 4$ for LHCb.

The results were presented first as $R_{p\rm Pb}(y)$, left-hand panel of Fig. 2, with an extrapolated pp normalization since there is no pp measurement at $\sqrt{s}$ = 5 TeV. The pp normalization is based on an interpolation between the pp measurements at $\sqrt{s}$ = 2.76 and 7 TeV, along with a model-based systematic uncertainty [5]. Note that ALICE presented both a single bin value of $R_{p\rm Pb}$ in the forward and backward regions as well as divided into six rapidity bins. In both rapidity regions, the ALICE points seem to be above the LHCb results. However, the data are compatible within the statistical uncertainties.

In addition, to eliminate the dependence on the uncertain pp normalization, a forward-backward production ratio, $R_{F/B}(y, \sqrt{s_{NN}}) = R_{p\rm Pb}(+|y|, \sqrt{s_{NN}})/R_{p\rm Pb}(-|y|, \sqrt{s_{NN}})$, was extracted where $R_{F/B}$ is defined with the proton beam moving toward positive y in the numerator and negative y in the denominator. Thus cold matter effects dominant at small x are in the numerator while the denominator probes larger x. The pp contributions to $R_{p\rm Pb}$ cancel in the ratio because pp collisions are symmetric around midrapidity. In both cases, the rapidity shift is taken into account to compare with calculations assuming no rapidity shift. The forward-backward ratio is shown as a function of rapidity and p_T in the center and right-hand panels of Fig. 2. The two measurements are in very good agreement within the region of overlap here, suggesting that the pp normalization is responsible for the difference seen in $R_{p\rm Pb}(y)$.

In addition to the J/ψ calculations in the color evaporation model at next-to-leading order in Ref. [1], calculations by Arleo and Peigné [8, 9] are also shown.

The NLO EPS09 band is obtained by calculating the deviations from the central value for the 15 parameter

variations on either side of the central set and adding them in quadrature (dashed histograms on the left-hand side of Fig. 2). With the new uncertainties on the charm cross section [10], the band obtained with the mass and scale variation (dot-dashed histograms on the left-hand side of Fig. 2) is narrower than that with the EPS09 variations. Only the nPDF variation is shown in the forward-backward ratios in the center and right-hand panels of Fig. 2. The NLO EPS09 band is narrower and exhibits less shadowing than the corresponding LO result.

The calculations by Arleo *et al.* are based on energy loss in cold nuclear matter, without and with the central EPS09 set. They fit an energy loss parameter, q_0, to the $\sqrt{s_{NN}}$ = 38.8 GeV E866 data and employ the same parameter for other energies. They find q_0 = 0.075 GeV^2/fm without shadowing and 0.055 GeV^2/fm with the EPS09 central parameter set. The rapidity distributions modified by the energy loss probability, $P(\epsilon)$, used to fit q_0 are defined as

$$\frac{1}{A}\frac{d\sigma_{pA}(y)}{dy} = \int_0^{\min(E,E_p-E)} d\epsilon P(\epsilon)\frac{E}{E+\epsilon}\frac{d\sigma_{pp}(y+\delta y(\epsilon))}{dy} \quad (1)$$

where E is the energy of the J/ψ in the rest frame of the nucleus. No specific J/ψ production model is assumed and instead a parameterization of the pp cross section, $d\sigma_{pp}/dp_T dx = [(1-x)^n/x][p_0^2/(p_0^2+p_T^2)]^m$, is adopted. The parameters n and m are fit to pp data. Due to the steep dependence of the gluon distribution on x, they find $n \sim 5$ at $\sqrt{s}$ = 38.8 GeV and 34 at 2.76 TeV. Including shadowing as well as energy loss reduces the fitted energy loss parameter. There is no significant difference in the shape of R_{pA} at fixed-target energies but they arise at higher $\sqrt{s}$. See Refs. [8, 9] for more details.

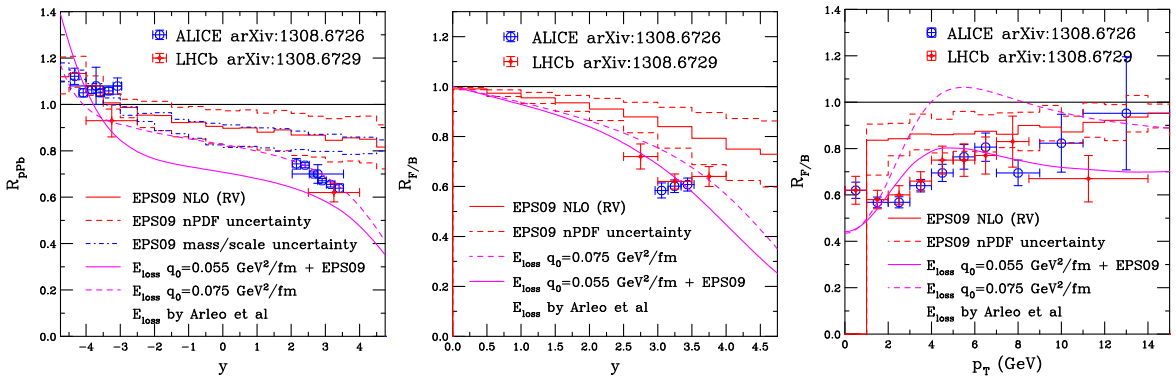

Figure 2. (Left) The $R_{p\mathrm{Pb}}$ ratio for J/ψ as a function of y. The dashed histogram shows the EPS09 uncertainties while the dot-dashed histogram shows the dependence on mass and scale. The pp denominator is also calculated at 5 TeV. The $R_{F/B}$ ratios for J/ψ as a function of y (center) and p_T (right). The dashed histogram shows the EPS09 uncertainties. The energy loss calculations of Arleo and Peigné are shown as smooth curves.

I thank J. Albacete, F. Arleo, A. Dumitru, F. Jing, Z. Lin, A. Rezaeian, C. Roland, E. Scomparin, P. Steinberg, J. Velkovska, and X.-N. Wang for comments and contributions. This work was performed under the auspices of the U.S. Department of Energy by Lawrence Livermore National Laboratory under Contract DE-AC52-07NA27344 and supported in part by the JET collaboration.

References

[1] J. L. Albacete *et al*, Int. J. Mod. Phys. E **22** (2013) 1330007.
[2] Z.-W. Lin, C. M. Ko, B.-A. Li, B. Zhang and S. Pal, Phys. Rev. C **72** (2005) 064901.
[3] A. H. Rezaeian, Phys. Lett. B **718** (2013) 1058.
[4] A. Milov *et al.* (ATLAS Collaboration), these proceedings.
[5] B. Abelev *et al.* (ALICE Collaboration), arXiv:1308.6726.
[6] R. Aaij *et al.* (LHCb Collaboration), arXiv:1308.6729.
[7] J. Albacete and A. Dumitru, private communication.
[8] F. Arleo and S. Peigné, JHEP **1303** (2013) 122.
[9] F. Arleo, R. Kolevatov, S. Peigné and M. Rustamova, JHEP **1305** (2013) 155.
[10] R. E. Nelson, R. Vogt and A. D. Frawley, Phys. Rev. C **87** (2013) 014908.